ACS APPLIED MATERIALS & INTERFACES

May 5, 2021
Volume 13
Number 17
pubs.acs.org/acsami

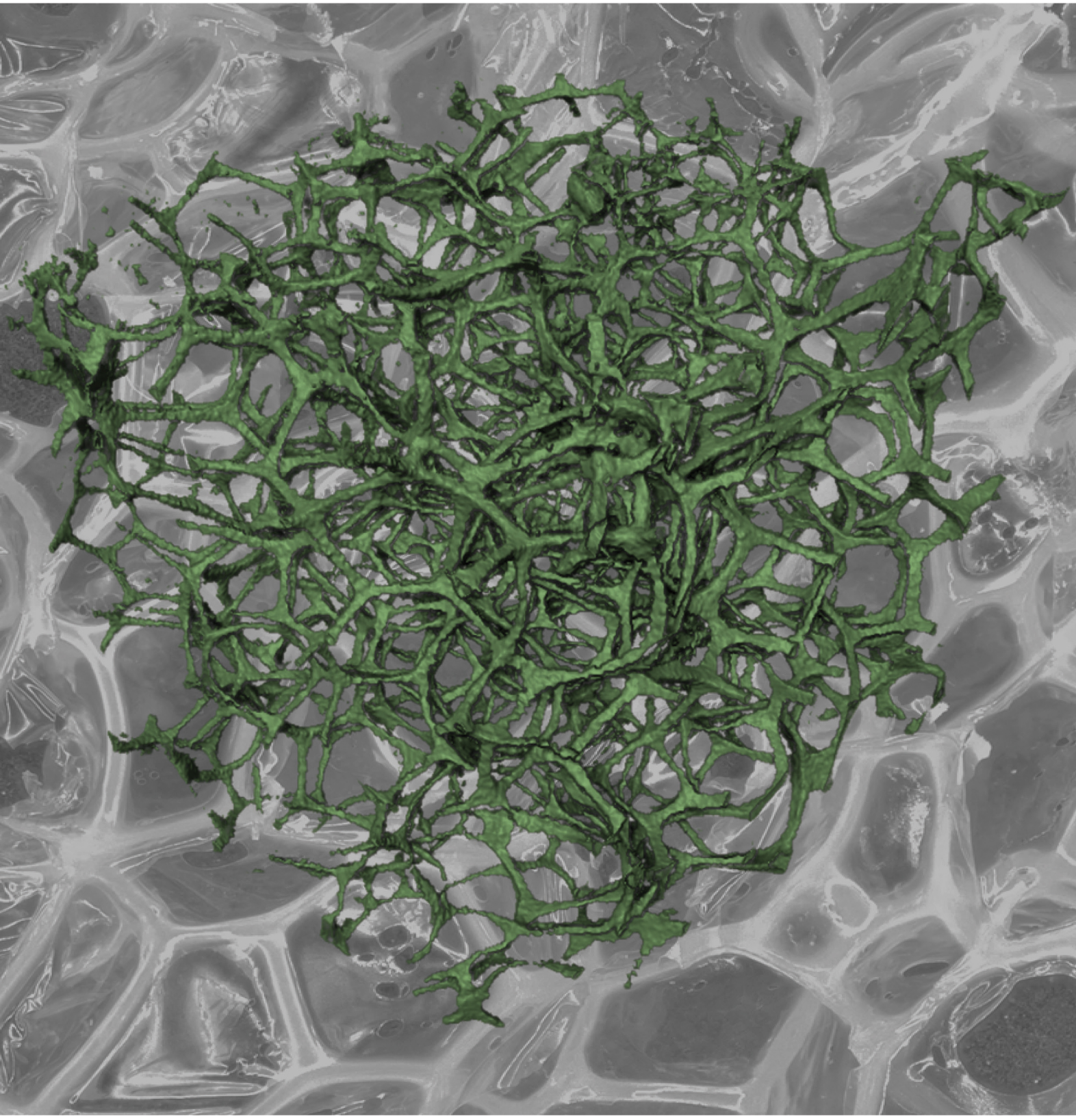

ACS Publications
Most Trusted. Most Cited. Most Read.

www.acs.org

ACS APPLIED MATERIALS & INTERFACES

www.acsami.org Research Article

Field-Free Deterministic Magnetization Switching Induced by Interlaced Spin−Orbit Torques

Min Wang, Zhaohao Wang,* Chao Wang, and Weisheng Zhao*

Cite This: *ACS Appl. Mater. Interfaces* 2021, 13, 20763−20769 Read Online

ACCESS | Metrics & More | Article Recommendations | Supporting Information

ABSTRACT: Spin−orbit torque (SOT) magnetic random access memory is envisioned as an emerging nonvolatile memory due to its ultrahigh speed and low power consumption. The field-free switching scheme in SOT devices is of great interest to both academia and industry. Here, we propose a novel field-free deterministic magnetization switching scheme in a regular magnetic tunnel junction by using two currents sequentially passing interlaced paths, with less requirements of the manufacturing process or additional physical effects. The switching is bipolar since the final magnetization state depends on the combination of current paths. The functionality and robustness of the proposed scheme are validated through both macrospin and micromagnetic simulation. The influences of field-like torque and the Dzyaloshinskii−Moriya interaction effect are further researched. Our proposed scheme shows good scalability and is expected to realize novel digital logic and even computing-in-memory platforms.

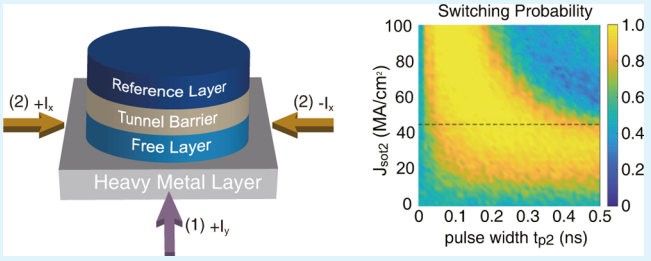

KEYWORDS: *spin−orbit torque, field-free switching, Dzyaloshinskii−Moriya interaction, domain-wall motion, micromagnetic simulation*

INTRODUCTION

Fast and energy-efficient switching of the perpendicular magnetization has attracted intensive research interest since it directly influences the application potential of spintronic devices such as magnetic tunnel junction (MTJ).[1,2] Currently, the spin-transfer torque (STT), as the mainstream technology in nonvolatile memory, is suffering from the bottlenecks of speed, energy, and reliability.[3−6] For instance, the intrinsic incubation delay of the STT limits the speed of magnetization switching. The charge current for inducing the STT directly flows through the MTJ and hence easily damages the tunnel barrier. To overcome these bottlenecks, the emerging spin−orbit torque (SOT) technology has been proposed and shows the advantages of higher speed, lower energy, and higher reliability.[7−15] Nonetheless, for achieving the deterministic switching of perpendicular magnetization, most of the SOT prototype devices have to be used in conjunction with an additional magnetic field,[16−18] which blocks the practical realization of the SOT-based circuits and architectures. Therefore, the field-free SOT switching scheme is drawing more and more attention on account of practical applications.

Until now, various methods of field-free SOT-induced switching have been reported, such as creating a lateral structural asymmetry via special fabrication process,[19,20] tilting the anisotropy,[21] adopting the antiferromagnetic layer with a strong SO coupling (SOC),[22−25] utilizing the spin current gradient,[26] adjusting the Dzyaloshinskii−Moriya interaction (DMI) effect[27−29] or field-like torque,[30] utilizing a circularly polarized AC current[31] or two time-dependent currents,[32] introducing shape anisotropy,[33,34] combining two orthogonal currents with partially overlapped SOC layers or shape anisotropy,[35,36] coupling two ferromagnetic layers with different types of anisotropy,[37,38] producing a lateral Pt gradient within the Co layer,[39] and so forth.[40−47] However, the majority of these methods bring out special requirements in the fabrication process or material type of the device. In addition, although two simultaneously applied AC currents or time-dependent currents could avoid the use of the magnetic field,[31,32] the generation of those currents is a challenge in practical application.

In this paper, we propose a novel SOT-based technology for achieving field-free deterministic switching of perpendicular magnetization. Two DC currents are applied consecutively, as the second current plays a dominating role in field-free switching. Compared with the existing methods, our proposal shows better feasibility. For instance, compared with ref 36, our scheme could be implemented in the regular circular SOT-MTJ and the regular-shaped heavy-metal (HM) layer, without the requirement of the special fabrication process or physical effects, which also brings the flexible combination of operational current paths. Furthermore, our proposal leads to

Received: December 31, 2020
Accepted: April 12, 2021
Published: April 22, 2021

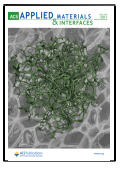

https://doi.org/10.1021/acsami.0c23127
ACS Appl. Mater. Interfaces 2021, 13, 20763−20769

bipolar switching, which could be naturally applied in the spintronic memories or computing circuits.

MODEL AND SIMULATION

The schematic structure of our proposed field-free device is illustrated in Figure 1. A regular MTJ is utilized, including a

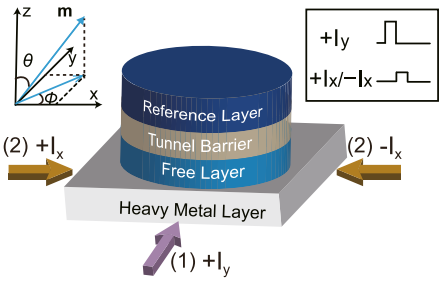

Figure 1. Schematic structure of the studied device, including the free layer, tunnel barrier, reference layer, and HM layer. The top-left is the coordinate system.

tunnel barrier sandwiched between two ferromagnetic layers, that is, free layer (FL) and reference layer (RL), fabricated above a HM layer. The magnetization of RL is fixed, while the magnetization of FL can be switched by current-induced SOT through the HM layer. Our scheme requires two current paths, that is, $\pm x$ axis and $\pm y$ axis, which can be achieved by adding four pins to the HM layer. In application, the NAND-like structure, where the multiple MTJ cells share the same HM layer, could be adopted to reduce the average number of pins of each bit-cell.[48] The magnetization dynamics of the FL can be described by a modified Landau−Lifshitz−Gilbert (LLG) equation[49,50]

$$\frac{\partial \boldsymbol{m}}{\partial t} = -\gamma\mu_0 \boldsymbol{m} \times \boldsymbol{H}_{\text{eff}} + \alpha \boldsymbol{m} \times \frac{\partial \boldsymbol{m}}{\partial t} + \boldsymbol{\tau}_{\text{DL}} + \boldsymbol{\tau}_{\text{FL}} \quad (1)$$

$$\boldsymbol{\tau}_{\text{DL}} = J_{\text{sot}} \xi \lambda_{\text{DL}} \boldsymbol{m} \times (\boldsymbol{\sigma} \times \boldsymbol{m}) \quad (2)$$

$$\boldsymbol{\tau}_{\text{FL}} = J_{\text{sot}} \xi \lambda_{\text{FL}} (\boldsymbol{\sigma} \times \boldsymbol{m}) \quad (3)$$

$$\xi = \frac{\gamma \hbar}{2 e t_{\text{F}} M_{\text{s}}} \quad (4)$$

where γ is the gyromagnetic ratio. μ_0 refers to the vacuum permeability. $\boldsymbol{\sigma}$ denotes the polarization vector of the SOT-induced spin injection. J_{sot} is the SOT current density. ξ is a device-dependent parameter. λ_{DL} and λ_{FL} reflect the magnitudes of damping-like torque and field-like torque, respectively. λ_{DL} is equivalent to the spin-Hall angle. Other parameters are listed in Table 1, which are consistent with the state-of-the-art technologies.

Table 1. Parameters of Simulation[27,51−53]

symbol	parameter	default value
	MTJ area	$0.25 \times \pi \times 70$ nm $\times$ 70 nm
t_{F}	thickness of FL	0.8 nm
α	damping constant	0.3
A_{ex}	exchange constant	1.6×10^{-11} J/m
K_{u}	magnetic anisotropy	8×10^5 J/m^3
M_{s}	saturation magnetization	1.1×10^6 A/m
θ_{sot}	spin Hall angle	0.3

The combinations of current $\{+I_y, +I_x\}$ and $\{+I_y, -I_x\}$ are chosen to achieve bipolar switching, as shown in Figure 1. In this choice, the first current is unidirectional, which helps to suppress the source degeneration effect of the access transistors and facilitates the application of diodes, leading to the reduction of the cell area. It should be noticed that two simultaneously applied DC SOT currents cannot induce the field-free deterministic magnetization switching[16,18] since the structure symmetry is not broken. Following is an exemplary switching process, which can be accomplished in two steps:

Step 1. A charge current in the $+y$ direction $(+I_y)$, with current density J_{sot1} and pulse width t_{p1}, is applied to the HM layer, inducing a spin current polarized along the $-x$ direction according to the spin-Hall effect. Thus, regardless of initial magnetization, the normalized magnetization vector $(\boldsymbol{m})$ is pulled to the $-x$ direction, that is, a metastable in-plane state, as shown in Figure 2.

Step 2. $+I_y$ is removed and subsequently the other current $(+I_x$ or $-I_x)$ is applied in the $+x$ or $-x$ direction, with current density J_{sot2} and pulse width t_{p2}. Starting from the metastable in-plane state, the magnetization switching could be achieved through two modes depending on the magnitude of J_{sot2}. On the one hand, if J_{sot2} is large enough, the magnetization first rotates toward the $-z$ or $+z$ axis under the action of $+I_x$ or $-I_x$ and then returns to the in-plane direction. In this case, the deterministic switching could be achieved as long as $+I_x$ or $-I_x$ is turned off before the magnetization significantly returns to the in-plane direction. This mechanism is named mode-I switching. The typical curves of time-dependent m_z and trajectories of the magnetization vector are shown in Figure 2a−d. On the other hand, if J_{sot2} is relatively weak, the magnetization could directly be switched to the $-z$ or $+z$ direction, even if $+I_x$ or $-I_x$ is not turned off. This mechanism is named mode-II switching, as shown in Figure 2e,f. Hereinafter, the current pulses applied in steps 1 and 2 are noted as "the first current" and "the second current", respectively.

Below, first we will focus on the influences of the current pulse parameters on the magnetization switching. Afterward, the robustness of our proposed scheme is studied. Finally, micromagnetic simulation is performed to reveal more features of the magnetic dynamics.

RESULTS AND DISCUSSION

The choice of current paths is not unique since the studied device has structure symmetry between x and y axes. Table 2 lists the feasible combinations of the current pulses for the bipolar switching. For instance, either of the currents can be set as a unidirectional current, benefiting the use of diodes as access transistors and thus reducing the bit-cell area. Furthermore, the combinations of $\{+I_y, -I_x\}$ and $\{-I_x, +I_y\}$ could be chosen, with two unidirectional currents, to write "+1" and "−1", respectively. In this case, note that the current density needs to be adjusted according to the polarity of the written data. It is observed in Table 2 that when the second current is in a clockwise (counterclockwise) relationship with the first current, magnetization will be switched to the $-z$ $(+z)$ direction. Therefore, in practical applications, the current combinations could be flexibly chosen, which provides the potential as logic devices.

Considering the symmetry among the various combinations, we will only analyze the case of {step 1: $+I_y$; step 2: $-I_x$} in this section and take the $-z$-to-$+z$ switching process as an example.

https://doi.org/10.1021/acsami.0c23127
ACS Appl. Mater. Interfaces 2021, 13, 20763−20769

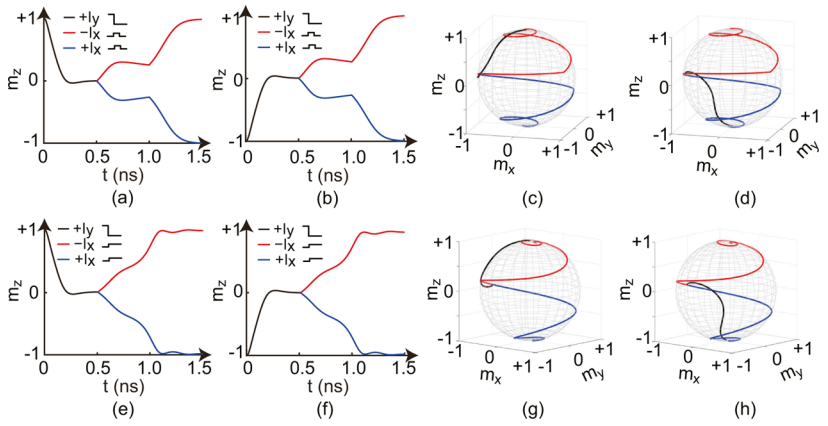

Figure 2. (a,b,e,f) Typical simulation results of time-dependent z-component magnetization (m_z) for (a,b) mode-I switching and (e,f) mode-II switching. (c,d,g,h) Trajectories of the magnetization vector for (c,d) mode-I switching and (g,h) mode-II switching. In all cases, the first current: J_{sot1} = 100 MA/cm^2, t_{p1} = 0.5 ns. The second current in (a−d), J_{sot2} = 30 MA/cm^2, t_{p2} = 0.5 ns, in (e,f), J_{sot2} = 20 MA/cm^2, t_{p2} = 1 ns.

Table 2. Feasible Combinations of Current Pulses

the first current	the second current	final state of m_z
$+I_y$	$+I_x$	−1
$+I_y$	$-I_x$	+1
$-I_y$	$+I_x$	+1
$-I_y$	$-I_x$	−1
$+I_x$	$+I_y$	+1
$+I_x$	$-I_y$	−1
$-I_x$	$+I_y$	−1
$-I_x$	$-I_y$	+1

In addition, as the first current is only responsible for driving the magnetization to the in-plane direction, we will mainly discuss the influence of the second current. Macrospin simulation is performed for the preliminary analysis. Then, the multidomain dynamics and DMI effect are discussed through micromagnetic simulation.

Influence of the Second Current. The second current ($-I_x$ in our example) plays a key role in the magnetization switching. As shown in Figure 2a−d, for mode-I switching, $-I_x$ must be removed at an appropriate time, otherwise the magnetization vector will be pulled to the in-plane direction again by the SOT. In order to obtain the optimal pulse width for mode-I switching, we show the curves of m_y and m_z during step 2 in Figure 3a. It is observed that the time corresponding to the extreme value of m_z ($m_{z,ex}$), that is, the optimal pulse width (t_o), can be estimated by the intersection between the tangent line of m_y at the initial time and the time axis. Through this method, the tangent line of m_y and the estimated value t_o for mode-I switching could be derived by solving the LLG equation in a spherical coordinate, as follows

$$\left.\frac{\partial m_y}{\partial t}\right|_{\theta_0=\pi/2,\phi_0=\pi} = -\frac{J_{sot2}\xi\theta_{sot}}{1+\alpha^2} \tag{5}$$

$$t_o = \frac{1+\alpha^2}{J_{sot2}\xi\theta_{sot}} \tag{6}$$

Figure 3b presents the results of the theoretically estimated t_o (solid line) and simulated t_o (points) in mode-I switching, where the accuracy is improved as current density increases. Furthermore, eq 6 correctly describes the parameter dependence of t_o on J_{sot2} and α, as shown in Figures 3b and S1. In addition to the positive correlation effect on t_o, a larger α can improve the reliability of mode-I switching, as shown in Figure 3c. A higher α could cause the larger $m_{z,ex}$ in the curve of m_z for mode-I switching, which can be reflected by the initial slope of m_z, estimated by

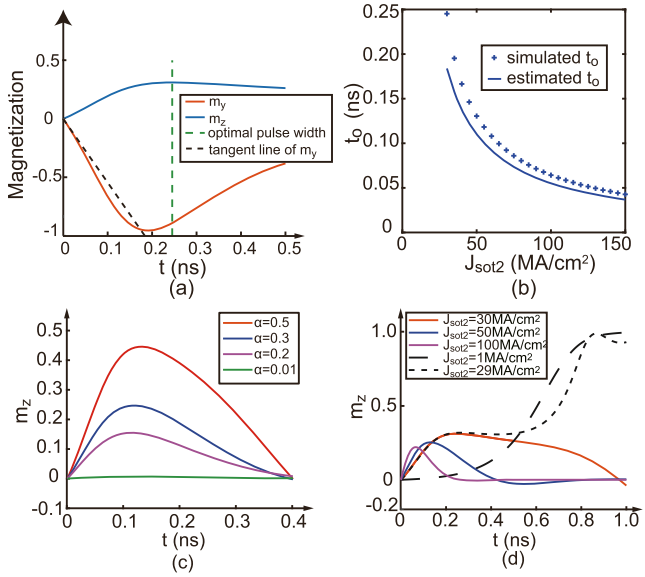

Figure 3. (a) Time evolution of m_y and m_z under the action of $-I_x$ in step 2. (b) Theoretically estimated t_o and simulated t_o in Mode-I switching as a function of J_{sot2}. Influence of (c) α and (d) J_{sot2} on the magnetization switching in step 2 without withdrawing the current. (c) J_{sot2} = 55 MA/cm^2 and (d) α = 0.3.

$$\left.\frac{\partial m_z}{\partial t}\right|_{\theta_0=\pi/2,\phi_0=\pi} = \frac{\alpha J_{sot2}\xi\theta_{sot}}{1+\alpha^2} \tag{7}$$

As mentioned above, the second current density (J_{sot2}) has a dramatic effect on the process of magnetization switching. For the mode-II switching, the second current is so weak that it cannot pull the magnetization back into the plane again, and the magnetization will directly approach the $+z$ axis, shown as the dotted lines in Figure 3d. For the mode-I switching, the curve of m_z, caused by the second current, shows an extreme value, shown as solid lines in Figure 3d. In this case, the J_{sot2} dependence of the m_z curve could be described by the above

https://doi.org/10.1021/acsami.0c23127
ACS Appl. Mater. Interfaces 2021, 13, 20763−20769

eqs 6 and 7. The critical current density for the boundary between two modes is defined as J_c. Suppose the boundary state, where the value of $m_{z,ex}$ is close to that of α and the $\partial m_z/\partial t = 0$; thus, the estimated J_c is calculated as

$$J_c = \frac{\alpha\gamma\mu_0\sqrt{1-\alpha^2}H_{eff}}{\sqrt{2}\xi\theta_{sot}}d_1 \quad (8)$$

where $d_1 = 1.1$ is a fitting factor. Numerical simulations demonstrate that this fitting factor fluctuates little with the changes of magnetic parameters, as shown in Figure S2.

According to the mathematical meaning, for mode-I switching, the product of eqs 6 and 7 is $m_{z,ex}$, numerically equals α. This conclusion is in good agreement with Figure 3c. Nevertheless, there still exists deviation between the values of $m_{z,ex}$ and α, as can be seen from Figure 3c. This deviation could be minimized, while the applied current density is set to J_c. In fact, $m_{z,ex}$ is also related to the current density, as shown in Figure 3d. In mode-I switching, the larger second current tends to drive the magnetization back into the plane quickly and thus the smaller $m_{z,ex}$.

Thermal Robustness. Furthermore, the thermal fluctuation at room temperature, that is, 300 K, is taken into consideration to evaluate the robustness of the proposed scheme. The method is described in eq S1. When the first current density is set to an appropriate value, the magnetization can be driven into the plane, in the presence of thermal disturbance, as shown in Figure S3. Afterward, we focus on the influences of the second pulse width, the second current density, and field-like torque.

Second Current Density and Pulse Width. Simulation results in Figure 4 illustrate the switching probability as a function of current density and pulse width of the second current at various damping constants. As expected, a current window for the robust switching (probability is close to 1) could be seen from both figures. This window could be well explained by the above analysis. The excessively small current, for example, 1 MA/cm^2, induces an insufficient torque which fails to drive the magnetization switching. The excessively large current tends to pull the magnetization to the metastable in-plane direction and deteriorates the robustness. The current window for the robust switching could be enlarged by increasing the damping constant since a larger damping constant leads to a larger $m_{z,ex}$. It is observed that the theoretically estimated t_o in eq 6 is well included in the switching window in Figure 4. Through simulation, both switching modes allow the time overlap of two current pulses, showing good feasibility in the circuit-level application. In applications, the existing design of circuits, for instance, self-terminate circuits, could be applied to improve the switching reliability at room temperature. Relevant results are shown in Figures S4−S6.

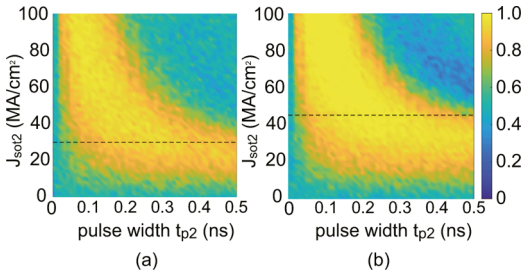

Figure 4. Switching probability in the down-to-up process as a function of the second current density and the second pulse width. (a) $\alpha = 0.3$ and (b) $\alpha = 0.5$. Dotted lines correspond to critical current density values in eq 8, with $d_1 = 1.1$.

Besides, referring to eq 6 and Figure 4, the energy consumption caused by the second current is estimated to be 7.7 and 8.9 fJ when α is 0.3 and 0.5, respectively. The total energy consumption is around 80 fJ after considering the first current (assume a 1 V power supply, $J_{sot1} = 100$ MA/cm^2, and $t_{p1} = 0.5$ ns). Therefore, the energy consumption of our proposal is comparable to the existing SOT switching schemes.

Field-like Torque. In this subsection, the influence of field-like torque on the magnetization switching is discussed. First, the magnetization behaviors with field-like torque at zero temperature are illustrated in Figure 5a,c. Then, the simulation results under thermal disturbance at 300 K are shown in Figure 5b,d. We found that mode-II switching could still occur in the presence of nonzero field-like torque, shown as the violet lines in Figure 5a,c. Below, we focus on the case of mode-I switching.

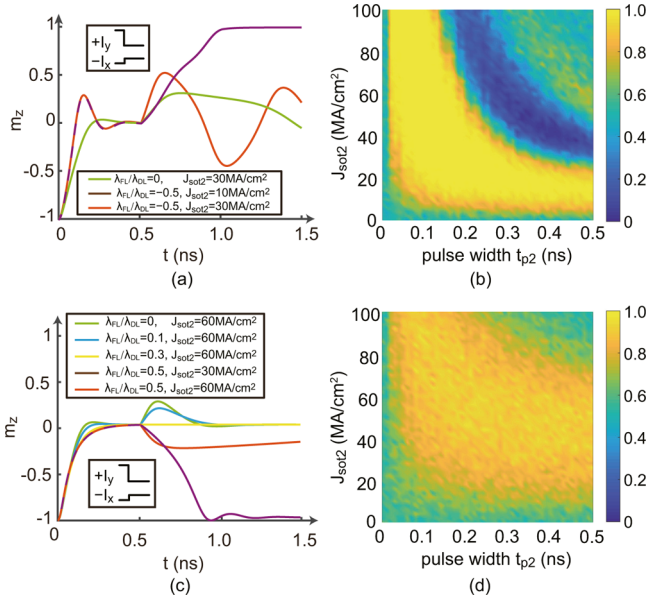

Figure 5. (a,c) Time-dependent m_z at 0 K with various field-like torques and second current densities. (b,d) Switching probability as a function of the second current density and pulse width at 300 K. (b) $\lambda_{FL}/\lambda_{DL} = -0.5$. (d) $\lambda_{FL}/\lambda_{DL} = 0.5$. In (a,b), $J_{sot1} = 100$ MA/cm^2. In (c,d), $J_{sot1} = 120$ MA/cm^2.

A negative field-like torque could cause the precession of m_z around the plane at zero temperature, shown as the red line in Figure 5a. Thus, the deterministic magnetization switching could be completed if the pulse width is set to an appropriate value. This inference is validated by Figure 5b, which shows the results of switching probability at room temperature. A window of pulse width for the robust switching is clearly seen. In addition, another window of pulse width for zero-probability switching is also seen, which is consistent with the precession behaviors shown in Figure 5a.

A positive field-like torque could decrease $m_{z,ex}$ and even reverse the polarity of magnetization switching (see Figure 5c). As to the switching probability at 300 K, referring to Figure 5d, a successful switching means final $-z$ magnetization since the

https://doi.org/10.1021/acsami.0c23127
ACS Appl. Mater. Interfaces 2021, 13, 20763−20769

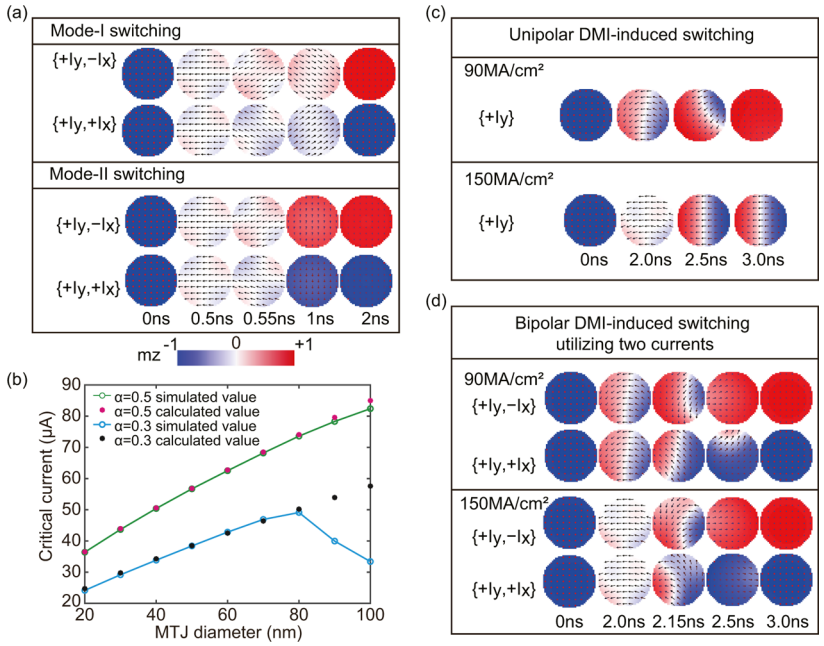

Figure 6. (a) Snapshots of time-dependent micromagnetic configurations for mode-I switching (J_{sot2} = 35 MA/cm^2, t_{p2} = 0.5 ns) and mode-II switching (J_{sot2} = 20 MA/cm^2, t_{p2} = 1.5 ns). (b) Critical value of the second current for two modes as a function of the MTJ diameter, with the thickness of the HM layer, t_{HM} = 2 nm. (c) Snapshots of magnetization during unipolar DMI-induced switching.[27] DMI magnitude: D = 0.5 mJ/m^2, t_{p1} = 2 ns. (d) Bipolar DMI-induced switching utilizing our proposal. J_{sot2} = 30 MA/cm^2, t_{p2} = 0.5 ns.

polarity of magnetization switching is reversed in the case of relatively large field-like torque. The reverse of the polarity means choosing the combination of current paths with the reverse relationship in Table 2. Compared with Figure 4a, the current window for robust switching in Figure 5d is greatly expanded; however, the switching probability in Figure 5d is smaller because of the decrease of $m_{z,ex}$.

Micromagnetic Simulation. Micromagnetic simulation was performed with the Object Oriented MicroMagnetic Framework[54] to reveal more details about the magnetization switching. The method is presented in eq S2. The mesh size is set to 2 nm × 2 nm × 0.8 nm. Typical results are shown in Figure 6a, where it can be seen that the magnetization switching is completed through the multidomain dynamics. All cases of switching are illustrated in Figures S7 and S8. Both mode-I and mode-II switching are achieved in the micromagnetic simulation. In both modes, the magnetic domains are configured to be at a balance state ($\langle m_z \rangle = 0$) at the end of the first current, while the second current is responsible for the deterministic switching. In mode-I switching, each magnetization will move to the $+z$ direction under the damping torque after withdrawing the current. In mode-II switching, the domain biased toward the $+z$ polarity will occupy the whole film under the action of the second current.

Critical Current in Microsimulation. Figure 6b depicts the micromagnetic simulation results of the critical second current between two modes versus the MTJ diameter. As the MTJ diameter decreases, the reduction in current and energy consumption show the potential for continuous scaling. By properly setting the fitting factor d_1 in eq 8, the theoretical value of the critical current is generally in agreement with the micromagnetic simulation results. Nevertheless, for α = 0.3, the deviation occurs when the MTJ diameter is larger, which might be attributed to the transformation from uniform switching to domain-governed switching.

DMI Effect. Recently, it was demonstrated that the combination of the DMI effect and SOT could lead to field-free magnetization switching.[27−29,55] The corresponding simulation results are shown in Figure 6c, where the current-induced SOT drives the domain wall across the midline, hence achieving deterministic switching in the presence of the DMI effect. However, the switching is unipolar, which might not be beneficial to the real circuit-level application since a read-before-write operation is required. In addition, the available operation window of current density for the deterministic switching is limited.

Our scheme could lead to bipolar switching even in the presence of the DMI effect, as shown in Figure 6d. The reason is that the direction of domain-wall motion depends on the polarity of the second current. Furthermore, our scheme relaxes the limit of the operation window of the first current since the final state is determined by the second current rather than the first current. Concerning both cases in Figure 6d, the domain walls are driven across the midline under the action of the second current, leading to deterministic switching.

CONCLUSIONS

We have proposed a novel scheme of field-free deterministic magnetization switching by utilizing interlaced SOT currents in a regular circular MTJ. Depending on the magnitude of the current density, two modes of bipolar switching were identified. The influences of key parameters on the magnetization switching were discussed through both macrospin and micromagnetic simulation. Theoretical models were deduced and showed good agreement with the simulation results. Compared with the existing field-free SOT scheme, our proposal could be implemented with a regular SOT-MTJ device, without the need for a special process or physical effects, showing great application potential in nonvolatile memory and logic computing.

https://doi.org/10.1021/acsami.0c23127
ACS Appl. Mater. Interfaces 2021, 13, 20763−20769

■ ASSOCIATED CONTENT

Supporting Information

The Supporting Information is available free of charge at https://pubs.acs.org/doi/10.1021/acsami.0c23127.

Numerical calculation and verification on eqs 6 and 8; statement of the fluctuating thermal field; phase diagram of the first current and switching probability; results of timing analysis; micromagnetic simulation method; and snapshots of magnetization (PDF)

■ AUTHOR INFORMATION

Corresponding Authors

Zhaohao Wang − *Fert Beijing Research Institute, MIIT Key Laboratory of Spintronics, School of Integrated Circuit Science and Engineering, Beihang University, Beijing 100191, China;* orcid.org/0000-0002-2999-7903; Email: zhaohao.wang@buaa.edu.cn

Weisheng Zhao − *Fert Beijing Research Institute, MIIT Key Laboratory of Spintronics, School of Integrated Circuit Science and Engineering, Beihang University, Beijing 100191, China;* orcid.org/0000-0001-8088-0404; Email: weisheng.zhao@buaa.edu.cn

Authors

Min Wang − *Fert Beijing Research Institute, MIIT Key Laboratory of Spintronics, School of Integrated Circuit Science and Engineering, Beihang University, Beijing 100191, China*

Chao Wang − *School of Electronics and Information Engineering, Beihang University, Beijing 100191, China*

Complete contact information is available at: https://pubs.acs.org/10.1021/acsami.0c23127

Notes

The authors declare no competing financial interest.

■ ACKNOWLEDGMENTS

This work was supported by the National Natural Science Foundation of China under Grant 61704005, the Beijing Municipal Science and Technology Project under Grant Z201100004220002, and the Fundamental Research Funds for the Central Universities under Grant YWF-20-BJ-J-1042.

■ REFERENCES

(1) Apalkov, D.; Dieny, B.; Slaughter, J. M. Magnetoresistive Random Access Memory. *Proc. IEEE* **2016**, *104*, 1796−1830.

(2) Bhatti, S.; Sbiaa, R.; Hirohata, A.; Ohno, H.; Fukami, S.; Piramanayagam, S. N. Spintronics Based Random Access Memory: A Review. *Mater. Today* **2017**, *20*, 530−548.

(3) Slonczewski, J. C. Current-Driven Excitation of Magnetic Multilayers. *J. Magn. Magn. Mater.* **1996**, *159*, L1−L7.

(4) Berger, L. Emission of Spin Waves by a Magnetic Multilayer Traversed by a Current. *Phys. Rev. B: Condens. Matter Mater. Phys.* **1996**, *54*, 9353.

(5) Brataas, A.; Kent, A. D.; Ohno, H. Current-Induced Torques in Magnetic Materials. *Nat. Mater.* **2012**, *11*, 372.

(6) Khvalkovskiy, A. V.; Apalkov, D.; Watts, S.; Chepulskii, R.; Beach, R. S.; Ong, A.; Tang, X.; Driskill-Smith, A.; Butler, W. H.; Visscher, P. B.; Lottis, D.; Chen, E.; Nikitin, V.; Krounbi, M. Basic Principles of STT-MRAM Cell Operation in Memory Arrays. *J. Phys. D: Appl. Phys.* **2013**, *46*, 074001.

(7) Ramaswamy, R.; Lee, J. M.; Cai, K.; Yang, H. Recent Advances in Spin-Orbit Torques: Moving Towards Device Applications. *Appl. Phys. Rev.* **2018**, *5*, 031107.

(8) Liu, L.; Pai, C.-F.; Li, Y.; Tseng, H. W.; Ralph, D. C.; Buhrman, R. A. Spin-Torque Switching with the Giant Spin Hall Effect of Tantalum. *Science* **2012**, *336*, 555−558.

(9) Cubukcu, M.; Boulle, O.; Drouard, M.; Garello, K.; Onur Avci, C.; Mihai Miron, I.; Langer, J.; Ocker, B.; Gambardella, P.; Gaudin, G. Spin-Orbit Torque Magnetization Switching of a Three-Terminal Perpendicular Magnetic Tunnel Junction. *Appl. Phys. Lett.* **2014**, *104*, 042406.

(10) Miron, I. M.; Moore, T.; Szambolics, H.; Buda-Prejbeanu, L. D.; Auffret, S.; Rodmacq, B.; Pizzini, S.; Vogel, J.; Bonfim, M.; Schuhl, A.; Gaudin, G. Fast Current-Induced Domain-Wall Motion Controlled by the Rashba Effect. *Nat. Mater.* **2011**, *10*, 419−423.

(11) Fukami, S.; Anekawa, T.; Zhang, C.; Ohno, H. A Spin-Orbit Torque Switching Scheme with Collinear Magnetic Easy Axis and Current Configuration. *Nat. Nanotechnol.* **2016**, *11*, 621−625.

(12) Lee, S.-W.; Lee, K.-J. Emerging Three-Terminal Magnetic Memory Devices. *Proc. IEEE* **2016**, *104*, 1831−1843.

(13) Wang, Z.; Li, Z.; Liu, Y.; Li, S.; Chang, L.; Kang, W.; Zhang, Y.; Zhao, W. Progresses and Challenges of Spin Orbit Torque Driven Magnetization Switching and Application. 2018 IEEE International Symposium on Circuits and Systems (ISCAS), 2018, pp 1−5.

(14) Lv, W.; Jia, Z.; Wang, B.; Lu, Y.; Luo, X.; Zhang, B.; Zeng, Z.; Liu, Z. Electric-Field Control of Spin-Orbit Torques in WS_2/Permalloy Bilayers. *ACS Appl. Mater. Interfaces* **2018**, *10*, 2843−2849.

(15) Chen, T.-Y.; Peng, C.-W.; Tsai, T.-Y.; Liao, W.-B.; Wu, C.-T.; Yen, H.-W.; Pai, C.-F. Efficient Spin-Orbit Torque Switching with Nonepitaxial Chalcogenide Heterostructures. *ACS Appl. Mater. Interfaces* **2020**, *12*, 7788−7794.

(16) Zhang, X.; Wan, C.; Yuan, Z.; Zhang, Q.; Wu, H.; Huang, L.; Kong, W.; Fang, C.; Khan, U.; Han, X. Electrical Control over Perpendicular Magnetization Switching Driven by Spin-Orbit Torques. *Phys. Rev. B* **2016**, *94*, 174434.

(17) Guo, C. Y.; Wan, C. H.; Zhao, M. K.; Wu, H.; Fang, C.; Yan, Z. R.; Feng, J. F.; Liu, H. F.; Han, X. F. Spin-Orbit Torque Switching in Perpendicular $Y_3Fe_5O_{12}$/Pt Bilayer. *Appl. Phys. Lett.* **2019**, *114*, 192409.

(18) Yang, W. L.; Wan, C. H.; Yan, Z. R.; Zhang, X.; Stebliy, M. E.; Wang, X.; Fang, C.; Guo, C.; Xing, Y. W.; Ma, T. Y.; Ognev, A. V.; Samardak, A. S.; Tung, M.-J.; Yu, G. Q.; Han, X. F. Chirality-Reversible Multistate Switching via Two Orthogonal Spin-Orbit Torques in a Perpendicularly Magnetized System. *Phys. Rev. Appl.* **2020**, *13*, 024052.

(19) Yu, G.; Upadhyaya, P.; Fan, Y.; Alzate, J. G.; Jiang, W.; Wong, K. L.; Takei, S.; Bender, S. A.; Chang, L.-T.; Jiang, Y.; Lang, M.; Tang, J.; Wang, Y.; Tserkovnyak, Y.; Amiri, P. K.; Wang, K. L. Switching of Perpendicular Magnetization by Spin-Orbit Torques in the Absence of External Magnetic Fields. *Nat. Nanotechnol.* **2014**, *9*, 548.

(20) Akyol, M.; Yu, G.; Alzate, J. G.; Upadhyaya, P.; Li, X.; Wong, K. L.; Ekicibil, A.; Khalili Amiri, P.; Wang, K. L. Current-Induced Spin-Orbit Torque Switching of Perpendicularly Magnetized Hf|CoFeB|MgO and Hf|CoFeB|TaOx Structures. *Appl. Phys. Lett.* **2015**, *106*, 162409.

(21) You, L.; Lee, O.; Bhowmik, D.; Labanowski, D.; Hong, J.; Bokor, J.; Salahuddin, S. Switching of Perpendicularly Polarized Nanomagnets with Spin Orbit Torque Without an External Magnetic Field by Engineering a Tilted Anisotropy. *Proc. Natl. Acad. Sci. U.S.A.* **2015**, *112*, 10310−10315.

(22) Fukami, S.; Zhang, C.; DuttaGupta, S.; Kurenkov, A.; Ohno, H. Magnetization Switching by Spin-Orbit Torque in an Antiferromagnet-Ferromagnet Bilayer System. *Nat. Mater.* **2016**, *15*, 535.

(23) Lau, Y.-C.; Betto, D.; Rode, K.; Coey, J. M. D.; Stamenov, P. Spin-Orbit Torque Switching Without an External Field Using Interlayer Exchange Coupling. *Nat. Nanotechnol.* **2016**, *11*, 758.

(24) Oh, Y.-W.; Chris Baek, S.-h.; Kim, Y. M.; Lee, H. Y.; Lee, K.-D.; Yang, C.-G.; Park, E.-S.; Lee, K.-S.; Kim, K.-W.; Go, G.; Jeong, J.-R.; Min, B.-C.; Lee, H.-W.; Lee, K.-J.; Park, B.-G. Field-Free Switching of Perpendicular Magnetization Through Spin-Orbit Torque in Antiferromagnet/ferromagnet/oxide Structures. *Nat. Nanotechnol.* **2016**, *11*, 878−884.

(25) van den Brink, A.; Vermijs, G.; Solignac, A.; Koo, J.; Kohlhepp, J. T.; Swagten, H. J.; Koopmans, B. Field-Free Magnetization Reversal by Spin-Hall Effect and Exchange Bias. *Nat. Commun.* **2016**, *7*, 10854.
(26) Chen, S.; Yu, J.; Xie, Q.; Zhang, X.; Lin, W.; Liu, L.; Zhou, J.; Shu, X.; Guo, R.; Zhang, Z.; Chen, J. Free Field Electric Switching of Perpendicularly Magnetized Thin Film by Spin Current Gradient. *ACS Appl. Mater. Interfaces* **2019**, *11*, 30446−30452.
(27) Chen, B.; Lourembam, J.; Goolaup, S.; Lim, S. T. Field-Free Spin-Orbit Torque Switching of a Perpendicular Ferromagnet with Dzyaloshinskii-Moriya Interaction. *Appl. Phys. Lett.* **2019**, *114*, 022401.
(28) Dai, M.; Hu, J.-M. Field-Free Spin−Orbit Torque Perpendicular Magnetization Switching in ultrathin Nanostructures. *npj Comput. Mater.* **2020**, *6*, 78.
(29) Wu, K.; Su, D.; Saha, R.; Wang, J.-P. Deterministic Field-Free Switching of a Perpendicularly Magnetized Ferromagnetic Layer via the Joint Effects of the Dzyaloshinskii-Moriya Interaction and Damping- and Field-Like Spin-Orbit Torques: An Appraisal. *J. Phys. D: Appl. Phys.* **2020**, *53*, 205002.
(30) Legrand, W.; Ramaswamy, R.; Mishra, R.; Yang, H. Coherent Subnanosecond Switching of Perpendicular Magnetization by the Fieldlike Spin-Orbit Torque Without an External Magnetic Field. *Phys. Rev. Appl.* **2015**, *3*, 064012.
(31) Go, G.; Lee, S.-J.; Lee, K.-J. Switching of Perpendicular Magnetization via AC Spin-Orbit Torque. *Phys. Rev. Appl.* **2018**, *10*, 034047.
(32) Zhang, Y.; Yuan, H. Y.; Wang, X. S.; Wang, X. R. Breaking the Current Density Threshold in Spin-Orbit-Torque Magnetic Random Access Memory. *Phys. Rev. B* **2018**, *97*, 144416.
(33) Wang, Z.; Li, Z.; Wang, M.; Wu, B.; Zhu, D.; Zhao, W. Field-Free Spin-Orbit-Torque Switching of Perpendicular Magnetization Aided by Uniaxial Shape Anisotropy. *Nanotechnology* **2019**, *30*, 375202.
(34) Shi, Y.; Chi, K.; Li, Z.; Zhang, W.; Xing, Y.; Meng, H.; Liu, B. Reconfigurable Spin Orbit Logic Device Using Asymmetric Dzyaloshinskii-Moriya Interaction. *Appl. Phys. Lett.* **2020**, *117*, 072401.
(35) de Orio, R. L.; Makarov, A.; Goes, W.; Ender, J.; Fiorentini, S.; Sverdlov, V. Two-Pulse Magnetic Field-free Switching Scheme for Perpendicular SOT-MRAM with a Symmetric Square Free Layer. *Phys. B* **2020**, *578*, 411743.
(36) de Orio, R. L.; Makarov, A.; Selberherr, S.; Goes, W.; Ender, J.; Fiorentini, S.; Sverdlov, V. Robust Magnetic Field-Free Switching of a Perpendicularly Magnetized Free Layer for SOT-MRAM. *Solid-State Electron.* **2020**, *168*, 107730.
(37) Wang, X.; Wan, C.; Kong, W.; Zhang, X.; Xing, Y.; Fang, C.; Tao, B.; Yang, W.; Huang, L.; Wu, H.; Irfan, M.; Han, X. Field-Free Programmable Spin Logics via Chirality-Reversible Spin-Orbit Torque Switching. *Adv. Mater.* **2018**, *30*, 1801318.
(38) Sheng, Y.; Edmonds, K. W.; Ma, X.; Zheng, H.; Wang, K. Adjustable Current-Induced Magnetization Switching Utilizing Interlayer Exchange Coupling. *Adv. Electron. Mater.* **2018**, *4*, 1800224.
(39) Cao, Y.; Sheng, Y.; Edmonds, K. W.; Ji, Y.; Zheng, H.; Wang, K. Deterministic Magnetization Switching Using Lateral Spin-Orbit Torque. *Adv. Mater.* **2020**, *32*, 1907929.
(40) Safeer, C. K.; Jué, E.; Lopez, A.; Buda-Prejbeanu, L.; Auffret, S.; Pizzini, S.; Boulle, O.; Miron, I. M.; Gaudin, G. Spin-Orbit Torque Magnetization Switching Controlled by Geometry. *Nat. Nanotechnol.* **2016**, *11*, 143−146.
(41) Deng, J.; Fong, X.; Liang, G. Electric-Field-Induced Three-Terminal pMTJ Switching in the Absence of an External Magnetic Field. *Appl. Phys. Lett.* **2018**, *112*, 252405.
(42) Kazemi, M.; Rowlands, G. E.; Shi, S.; Buhrman, R. A.; Friedman, E. G. All-Spin-Orbit Switching of Perpendicular Magnetization. *IEEE Trans. Electron Devices* **2016**, *63*, 4499−4505.
(43) Wang, M.; Cai, W.; Zhu, D.; Wang, Z.; Kan, J.; Zhao, Z.; Cao, K.; Wang, Z.; Zhang, Y.; Zhang, T.; Park, C.; Wang, J.-P.; Fert, A.; Zhao, W. Field-Free Switching of a Perpendicular Magnetic Tunnel Junction Through the Interplay of Spin-Orbit and Spin-Transfer Torques. *Nat. Electron.* **2018**, *1*, 582−588.
(44) Sato, N.; Xue, F.; White, R. M.; Bi, C.; Wang, S. X. Two-Terminal Spin-Orbit Torque Magnetoresistive Random Access Memory. *Nat. Electron.* **2018**, *1*, 508−511.
(45) Cai, K.; Yang, M.; Ju, H.; Wang, S.; Ji, Y.; Li, B.; Edmonds, K. W.; Sheng, Y.; Zhang, B.; Zhang, N.; Liu, S.; Zheng, H.; Wang, K. Electric Field Control of Deterministic Current-Induced Magnetization Switching in a Hybrid Ferromagnetic/ferroelectric Structure. *Nat. Mater.* **2017**, *16*, 712−716.
(46) Lee, J. M.; Cai, K.; Yang, G.; Liu, Y.; Ramaswamy, R.; He, P.; Yang, H. Field-Free Spin-Orbit Torque Switching from Geometrical Domain-Wall Pinning. *Nano Lett.* **2018**, *18*, 4669−4674.
(47) Li, H.; Wang, G.; Li, D.; Hu, P.; Zhou, W.; Dang, S.; Ma, X.; Dai, T.; Kang, S.; Yu, F.; Zhou, X.; Wu, S.; Li, S. Field-Free Deterministic Magnetization Switching with Ultralow Current Density in Epitaxial Au/Fe_4N Bilayer Films. *ACS Appl. Mater. Interfaces* **2019**, *11*, 16965−16971.
(48) Zhou, H.; Wang, C.; Li, Z.; Wang, Z.; Liu, T.; Wu, B.; Zhao, W. Design of an Erasable Spintronics Memory Based on Current-Path-Dependent Field-Free Spin Orbit Torque. *AIP Adv.* **2020**, *10*, 015317.
(49) Landau, L.; Lifshtz, E. On the Theory of the Dispersion of Magnetic Permeability in Ferromagnetic Bodies. *Phys. Z. Sowjetunion* **1935**, *8*, 153−159.
(50) Gilbert, T. L. A Lagrangian Formulation of the Gyromagnetic Equation of the Magnetization Field. *Phys. Rev.* **1955**, *100*, 1243.
(51) Metaxas, P.; Jamet, J.; Mougin, A.; Cormier, M.; Ferré, J.; Baltz, V.; Rodmacq, B.; Dieny, B.; Stamps, R. Creep and Flow Regimes of Magnetic Domain-Wall Motion in Ultrathin Pt/Co/Pt Films with Perpendicular Anisotropy. *Phys. Rev. Lett.* **2007**, *99*, 217208.
(52) Liu, J.; Ohkubo, T.; Mitani, S.; Hono, K.; Hayashi, M. Correlation Between the Spin Hall Angle and the Structural Phases of Early 5d Transition Metals. *Appl. Phys. Lett.* **2015**, *107*, 232408.
(53) Pai, C.-F.; Liu, L.; Li, Y.; Tseng, H. W.; Ralph, D. C.; Buhrman, R. A. Spin Transfer Torque Devices Utilizing the Giant Spin Hall Effect of Tungsten. *Appl. Phys. Lett.* **2012**, *101*, 122404.
(54) Donahue, M. J.; Donahue, M. *OOMMF User's Guide*, version 1.0; US Department of Commerce, National Institute of Standards and Technology, 1999.
(55) Wang, M.; Wang, Z.; Zhang, X.; Zhao, W. Theoretical Conditions for Field-free Magnetization Switching Induced by Spin-orbit Torque and Dzyaloshinskii-Moriya Interaction. *IEEE Electron Device Lett.* **2021**, *42*, 148−151.

https://doi.org/10.1021/acsami.0c23127
ACS Appl. Mater. Interfaces 2021, 13, 20763−20769